

# Hydrodynamic Derivatives Investigation on Unconventionally Arranged Pusher-Barge Systems

Koh Kho King<sup>1</sup>, Hironori Yasukawa<sup>2</sup> and Noritaka Hirata<sup>3</sup>

<sup>1</sup>Ph.D course student, E-mail: khoking@gmail.com

<sup>2</sup>Professor, E-mail: yasukawa@naoe.hiroshima-u.ac.jp

<sup>3</sup>Assistant Professor, E-mail: nhirata@naoe.hiroshima-u.ac.jp

**Correspondence Address:**

Graduate School of Engineering,

Hiroshima University, 1-4-1 Kagamiyama, Higashi Hiroshima, Japan 739-8527.

Tel: +81-(0)82-422-7505

## Abstract

Unconventional arrangement of pusher-barge systems were studied in this paper. Pusher-barge systems consisted of 4 barges, 6 barges and 8 barges with one pusher were tested in various combinations. Captive model test was performed on the various combinations at Hiroshima University Towing Tank. Hydrodynamic derivatives of the systems were obtained from the model test data by using least square analysis method. For asymmetry condition, hydrodynamic derivatives  $Y'_0$ ,  $Y'_{\beta\beta}$ ,  $N'_0$ , and  $N'_{\beta\beta}$  were added in force and moment equations in order to get better fitting of the least square curves. Motion equations were modified to cover the asymmetry cases of pusher-barge system with lateral force and yaw moment due to the asymmetry arrangement included. Turning simulations (with 20 degrees in sudden angle change) were carried out and the comparison of advance distance and tactical diameter were made.

**Key words:** pusher-barge, unconventional arrangement, hydrodynamic derivatives, simulation

## 1 Introduction

Barge transportation has been in rapid growth in the recent years due to the demand of coal mining and transporting. With relatively spacious design and low operating cost, barge has been the preferred mean of transportation for transporting large quantity of cargo. Multiple barges tied together and moved by a pusher have been a popular practice in many countries, including in Asia: the Kapuas River in Kalimantan (Indonesia), Rejang River in Sarawak (Malaysia) and Mekong River in Laos. River width restriction is the main concern when choosing the suitable combination of pusher-barge system.

Nine different combinations of pusher-barges system arranged symmetrically port and starboard have been studied by the authors [1][2]. At times, the combination of pusher-barge systems might not favor to be in the conventional arrangement, due to the cargo type and size, and sea transportation law of a country. As a continuous study to the pusher-barge transportation, unconventional arrangement of pusher-barge system was tested in Hiroshima University Towing Tank. Eight different combinations of the pusher-barge system were tested, with pusher located either at the aft or side of the barges. An example of pusher-barge system during model test is shown in Figure 1.

## 2 Pusher-Barge System

With refer to Pfenningstorf's paper [3], a pusher with twin screws and twin rudders was designed and tested at Hiroshima University Towing Tank, together with the various combinations of barges. Two types of barges were designed: rake-barge and box-barge. Rake-barge is always the leading barge with rounded bow and box-barge is the in-between or aft barge. Body plan of the pusher and rake-barge are shown in Figure 2 and 3, and principal dimensions of the pusher and barges are shown in Table 1. The designed pusher has two controllable pitch propellers (CPP) with diameter ( $D_P$ ) 1.8m, revolution 300rpm and main

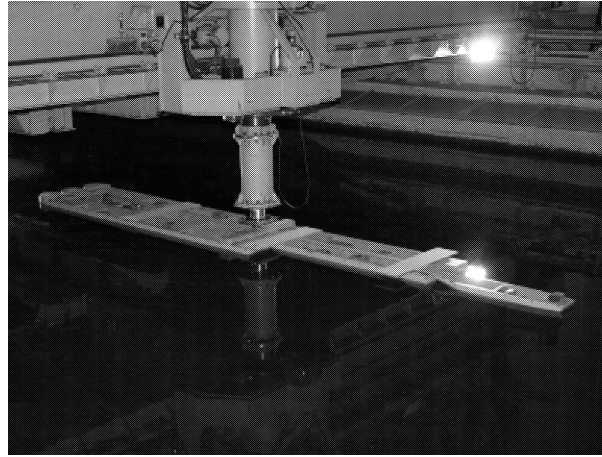


Figure 1: Pusher-barge 8BP(1) during model test

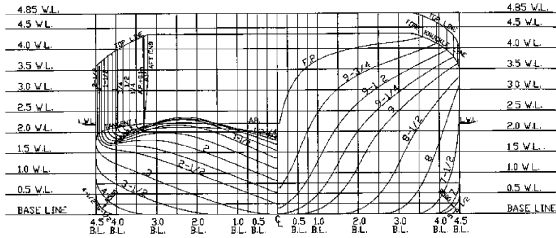


Figure 2: Body plan of the pusher

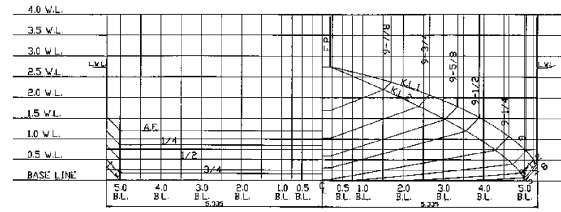


Figure 3: Body plan of the rake-barge

engine power 1340ps. Rudders used in the pusher are having span = 2.0m, cord = 2.0m and area = 4.0m<sup>2</sup> each.

Eight different combinations of the pusher-barge systems were designed. Among them, pusher-barge 4BP(1), 6BP(1) and 6BP(2) are conventional type and their performance and characteristics have been presented [1]. Pusher-barge 4BP(2), 6BP(3), 8BP(1), 8BP(2), and 8BP(3) are new unconventional types, with 8BP(1) and 8BP(2) are having asymmetry port and starboard arrangement. Pusher-barge 4BP(2), 8BP(2) and 8BP(3) have the pusher located in-between the barges while others are all having pusher located at the aft of the system. Figure 4 shows the designation of the various combinations of the pusher-barge systems and their principal particulars are shown in Table 2. In Table 2, LOA is the length overall of the pusher-barge system from the foremost part of the system to the farthest aft of the system.

Table 1: Principal dimensions of pusher, rake-barge and box-barge in full scale and model scale during experiment conditions

	pusher		box-barge		rake-barge	
	Full-scale	Model	Full-scale	Model	Full-scale	Model
Length overall, LOA (m)	40.0	0.80	60.96	1.219	60.96	1.219
Length btw. perpendiculars, LBP (m)	39.50	0.79	60.96	1.219	60.96	1.219
Breadth, $B$ (m)	9.00	0.18	10.67	0.213	10.67	0.213
Draught, $d$ (m)	2.2	0.044	2.74	0.0548	2.74	0.0548
Volume, $\nabla$ (m <sup>3</sup> )	494.7	0.00396	1707.6	0.01366	1646.2	0.01317
LCB from AP (m)	21.98	0.4395	30.48	0.6096	29.44	0.5888
Block coefficient, $C_b$	0.633	0.633	0.958	0.958	0.924	0.924

Table 2: Principal dimensions of pusher-barge systems in fullscale

symbol	4BP(1)	4BP(2)	6BP(1)	6BP(2)	6BP(3)	8BP(1)	8BP(2)	8BP(3)
LOA (m)	161.92	121.92	222.88	161.92	222.88	222.88	182.88	182.88
$B$ (m)	21.34	30.34	21.34	32.01	32.01	32.01	32.01	32.01
$d$ (m)	2.74	2.74	2.74	2.74	2.74	2.74	2.74	2.74
$\nabla$ (m <sup>3</sup> )	7202	7202	10618	10556	10679	13971	13971	13971
LCB from AP (m)	94.54	58.73	125.30	96.24	105.86	133.84	96.00	96.00
$C_b$	0.761	0.711	0.815	0.743	0.546	0.715	0.871	0.871

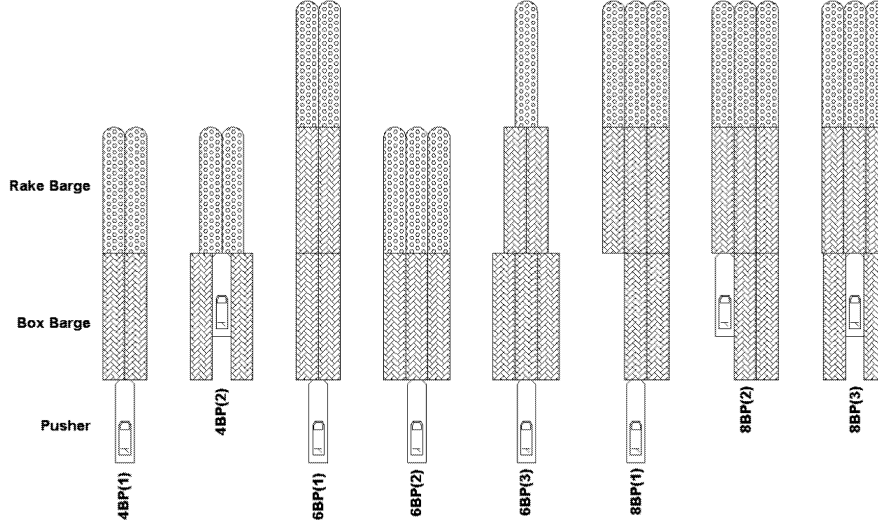


Figure 4: Pusher-barge systems in eight different combinations

### 3 Hydrodynamic Characteristics

#### 3.1 Model Test Outline

Circular Motion Test (CMT) was carried out at Hiroshima University Towing Tank (100m length  $\times$  7m width  $\times$  4m depth). Pusher and barges model were built at scale 1/50 and each pusher-barge system was tested at the corresponding full scale speed of 7 knots and draught 2.74m. During the test, the model was restrained from roll and heave motions but free to trim. Force and moment transducer was put at the midship of the pusher-barge system (exactly half of the total length of the pusher + barges). Longitudinal force ( $X_H^*$ ), lateral force ( $Y_H^*$ ) and yawing moment ( $N_H$ ) were measured and are then non-dimensionalised using the following equations:

$$X_H^*, Y_H^* = \frac{X_H^*, Y_H^*}{(1/2)\rho LOA dU^2} \quad (1)$$

$$N_H' = \frac{N_H}{(1/2)\rho LOA^2 dU^2} \quad (2)$$

where LOA is the length overall of pusher-barge system,  $\rho$  is the water density,  $d$  is the draught, and  $U$  is the ship speed. Figures 6 to 8 show the plot of the non-dimensional longitudinal and lateral forces and yawing moment around midship from the model tests. Forces measured from the model tests were having virtual masses of ship included. A more precise representation of the forces is shown below:

$$X_H^{*'} = X_H' - (m' + m'_y)r' \sin \beta_m \quad (3)$$

$$Y_H^{*'} = Y_H' - (m' + m'_x)r' \cos \beta_m \quad (4)$$

where,  $\beta_m$  is the drift angle at midship,  $r'$  is the non-dimensional value of the yaw rate ( $r' \equiv r \text{ LOA}/U$ ),  $X'_H$  and  $Y'_H$  are the hydrodynamic forces of the pusher-barge model without virtual masses of ship, and  $m$ ,  $m_x$  and  $m_y$  are the non-dimensional mass value with the following definition:

$$m', m'_x, m'_y = \frac{m, m_x, m_y}{(1/2)\rho \text{ LOA}^2 d} \quad (5)$$

### 3.2 Hydrodynamic Derivatives Equations Evaluation

Hydrodynamic derivatives equations as presented by the authors [1][2] are good for symmetrically arranged pusher-barge systems (Equation (6)). In order to represent the actual model test data more accurately for asymmetrically arranged pusher-barge systems, four new hydrodynamic derivative terms ( $Y_0$ ,  $Y'_{\beta\beta}$ ,  $N_0$ , and  $N'_{\beta\beta}$ ) were introduced. The new hydrodynamic derivatives equations are shown in Equation (7).

$$\left. \begin{aligned} X'_H &= X'_0 \cos^2 \beta_m + X'_{\beta\beta} \beta_m^2 + X'_{\beta r} \beta_m r' + X'_{rr} r'^2 \\ Y'_H &= Y'_\beta \beta_m + Y'_r r' + Y'_{\beta\beta\beta} \beta_m^3 + Y'_{\beta\beta r} \beta_m^2 r' \\ N'_H &= N'_\beta \beta_m + N'_r r' + N'_{\beta\beta\beta} \beta_m^3 + N'_{\beta\beta r} \beta_m^2 r' \end{aligned} \right\} \quad (6)$$

$$\left. \begin{aligned} X'_H &= X'_0 \cos^2 \beta_m + X'_{\beta\beta} \beta_m^2 + X'_{\beta r} \beta_m r' + X'_{rr} r'^2 \\ Y'_H &= Y'_0 + Y'_\beta \beta_m + Y'_r r' + Y'_{\beta\beta\beta} \beta_m^3 + Y'_{\beta\beta r} \beta_m^2 r' + Y'_{\beta\beta} \beta_m^2 \\ N'_H &= N'_0 + N'_\beta \beta_m + N'_r r' + N'_{\beta\beta\beta} \beta_m^3 + N'_{\beta\beta r} \beta_m^2 r' + N'_{\beta\beta} \beta_m^2 \end{aligned} \right\} \quad (7)$$

In the equations,  $X'_0$  is the forward resistance coefficient,  $X'_{\beta\beta}$ ,  $X'_{\beta r}$ , etc. are the hydrodynamic derivatives on maneuvering. For symmetrically arranged pusher-barge systems,  $Y'_0$ ,  $N'_0$ ,  $Y'_{\beta\beta}$ ,  $N'_{\beta\beta}$  are equal to zero.  $Y'_{\beta r r}$ ,  $Y'_{r r r}$ ,  $N'_{\beta r r}$ , and  $N'_{r r r}$  were eliminated as in the circular motion tests, at  $r' = 0.2$ , high accuracy for larger power of  $r'$  is hard to achieve [2]. For pusher-barge 8BP(1) and 8BP(2), it is found that by using Equation (7), it gives better curve fitting to the experiment data. Figure 5 shows the comparison of the asymmetrically arranged pusher-barge systems (8BP(1) and 8BP(2)) using equations (6) and (7) for  $Y'_H$  and  $N'_H$  curves. From the figure, it can be seen that Equation (7) gives better fitting on the  $N'_H$  curves for asymmetrically arranged pusher-barge systems, while  $Y'_H$  curves are similar in both equations.

### 3.3 Hydrodynamic Derivatives Discussions

Resistance coefficient and hydrodynamic derivatives on maneuvering captured from the model tests are shown in Table 3. Figures 6 to 8 show the least-square fitting using Equation (7) for both symmetrically and asymmetrically arranged pusher-barge systems. In view of practical use, the fitting is of satisfaction.

Course stability index,  $C$ , is included in Table 3 as well, with the following definition (rudder effect is not taking into account):

$$C = \frac{N'_r}{Y'_r - m' - m'_x} - \frac{N'_\beta}{Y'_\beta} \quad (8)$$

From Table 3, it can be seen that pusher-barge 4BP(2), 8BP(2) and 8BP(3) with pusher located in-between the barges and are not positioned at the farthest aft of the system, have negative value of  $C$ , which means unstable in course keeping.

## 4 Added Mass Coefficients

In this paper, added mass coefficients were calculated using singularity distribution method under the assumption of a rigid free-surface. Designation  $m_{ij}$  was used where  $i$  represents the direction and  $j$  is the motion mode of a specific added mass:  $i, j=1$  for surging motion;  $i, j=2$  for swaying motion;  $i, j=6$  for yawing motion.  $m'_{11}$ ,  $m'_{22}$ ,  $m'_{66}$  represent  $m'_x$ ,  $m'_y$ ,  $J'_{zz}$ . Table 4 shows the value of added mass coefficients for all the eight pusher-barge systems. For symmetrically arranged pusher-barge systems,  $m'_{12}$  and  $m'_{16}$  are equal to zero. For asymmetrically arranged pusher-barge systems, the effect of uneven lateral force and yaw moment in added mass needs to be taken into account. Maneuvering simulation conducted in this paper includes all added mass coefficients.

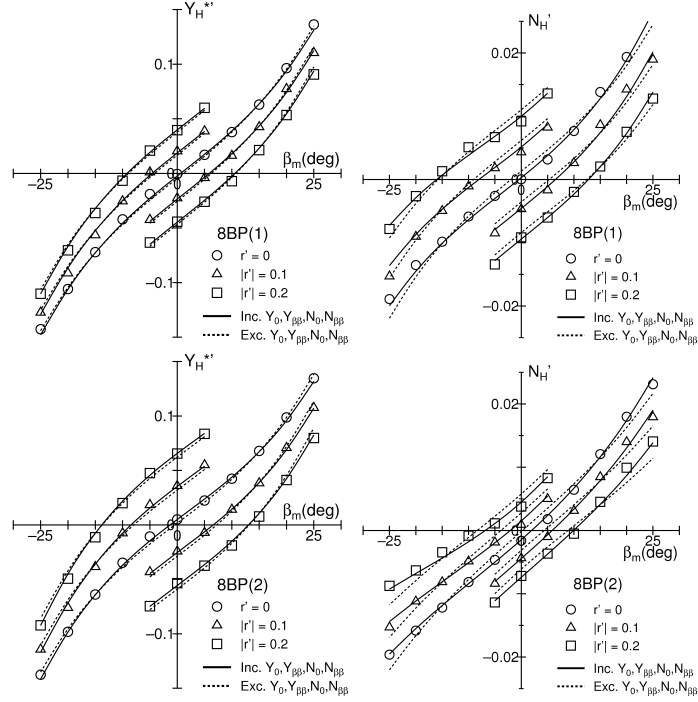


Figure 5: Fitting comparison of  $Y_H^{*'}$  and  $N_H'$  for 8BP(1) and 8BP(2) with and without  $Y_0, Y'_{\beta\beta}, N_0, N'_{\beta\beta}$

Table 3: Resistance coefficient, hydrodynamic derivatives on maneuvering and course stability index

symbol	4BP(1)	4BP(2)	6BP(1)	6BP(2)	6BP(3)	8BP(1)	8BP(2)	8BP(3)
$X'_0$	-0.0642	-0.1049	-0.0566	-0.0858	-0.0763	-0.0765	-0.0846	-0.0850
$X'_{\beta\beta}$	-0.0609	-0.1074	-0.0856	-0.0661	-0.0928	-0.0934	-0.0982	-0.1337
$X'_{rr}$	-0.0085	0.0124	0.0446	0.1128	-0.0064	0.0443	-0.0538	0.0293
$X'_{\beta r} - m'_y$	-0.1130	-0.2032	-0.0789	-0.1004	-0.0961	-0.0898	-0.1302	-0.1541
$Y'_0$	0.0	0.0	0.0	0.0	0.0	-0.0024	0.0050	0.0
$Y'_\beta$	0.2544	0.3292	0.2190	0.2442	0.2371	0.2272	0.2161	0.2519
$Y'_r - m'_x$	0.0122	0.0354	-0.0477	0.0137	0.0098	-0.0060	0.0016	0.0130
$Y'_{\beta\beta\beta}$	0.2795	0.7592	0.4809	0.4957	0.4972	0.4857	0.5105	0.6269
$Y'_{\beta\beta r}$	-0.0777	0.4937	-0.4078	0.1332	0.1064	0.1240	0.2993	0.4497
$Y'_{\beta\beta}$	0.0	0.0	0.0	0.0	0.0	-0.0309	-0.0517	0.0
$N'_0$	0.0	0.0	0.0	0.0	0.0	0.0003	-0.0015	0.0
$N'_\beta$	0.0397	0.0561	0.0308	0.0517	0.0298	0.0384	0.0420	0.0338
$N'_r$	-0.0497	-0.0297	-0.0422	-0.0756	-0.0214	-0.0485	-0.0297	-0.0319
$N'_{\beta\beta\beta}$	0.1381	0.0149	0.1291	0.1137	0.0769	0.0779	0.0424	-0.0020
$N'_{\beta\beta r}$	-0.0789	-0.5045	-0.1791	-0.0989	-0.1045	-0.0785	-0.1140	-0.1753
$N'_{\beta\beta}$	0.0	0.0	0.0	0.0	0.0	0.0158	0.0198	0.0
$C$	0.1079	-0.0769	0.0663	0.0578	0.0197	0.0607	-0.0964	-0.0247

Table 4: Added mass coefficients

symbol	4BP(1)	4BP(2)	6BP(1)	6BP(2)	6BP(3)	8BP(1)	8BP(2)	8BP(3)
$m'_x(m'_x)$	0.00760	0.01760	0.00437	0.01300	0.00589	0.00685	0.01064	0.01025
$m'_y(m'_y)$	0.07410	0.14040	0.05740	0.07870	0.05594	0.05984	0.08183	0.09414
$m'_{66}(J'_{zz})$	0.00430	0.01050	0.00363	0.00446	0.00364	0.00385	0.00610	0.00793
$m'_{26}$	-0.00127	-0.00542	-0.00069	-0.00175	0.00330	-0.00251	-0.00145	-0.00609
$m'_{12}$	0.0	0.0	0.0	0.0	0.0	0.00048	0.00104	0.0
$m'_{16}$	0.0	0.0	0.0	0.0	0.0	-0.00003	-0.00035	0.0

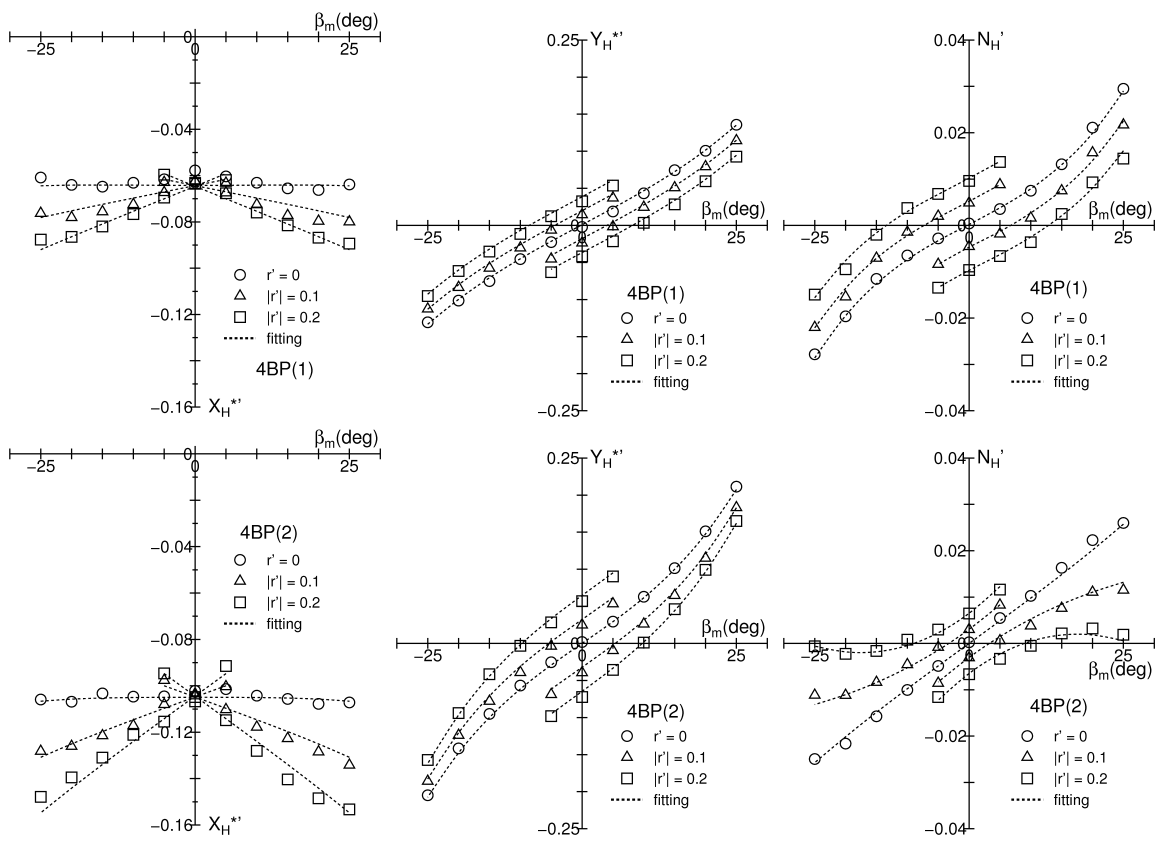


Figure 6: Measured force and moment coefficients for 4BP(1) and 4BP(2)

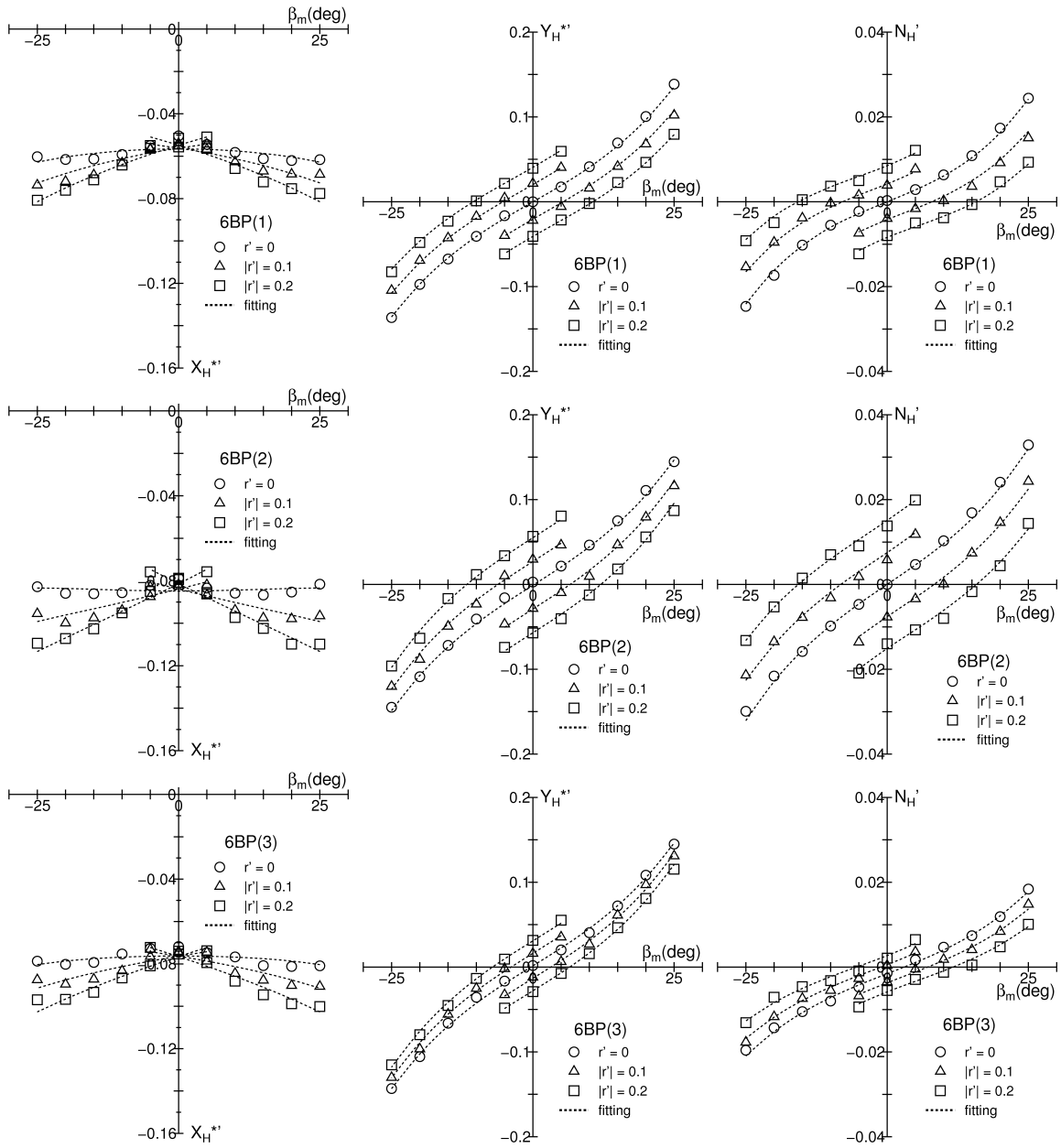


Figure 7: Measured force and moment coefficients for 6BP(1), 6BP(2), and 6BP(3)

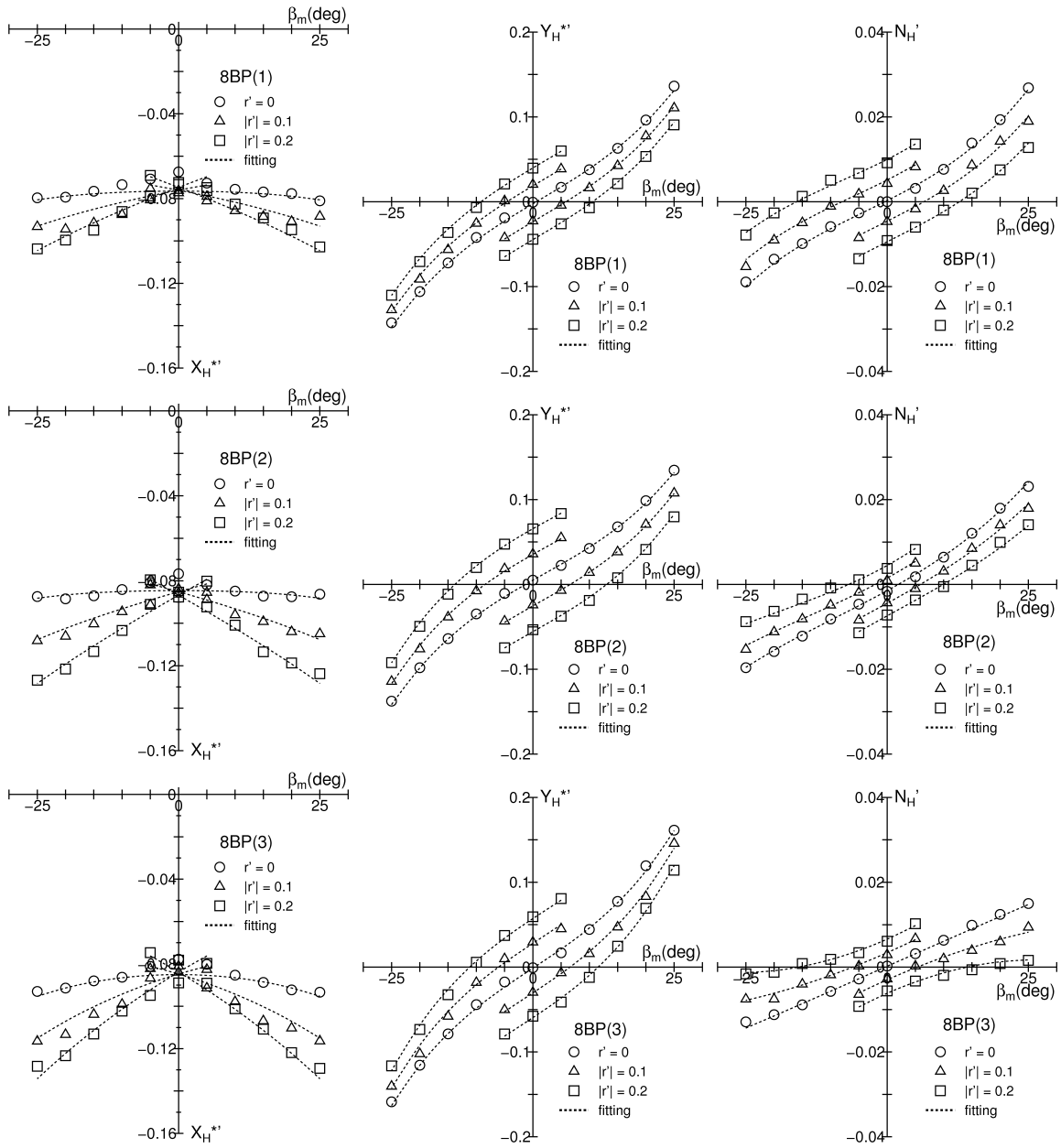


Figure 8: Measured force and moment coefficients for 8BP(1), 8BP(2), and 8BP(3)

## 5 Effective Power

Full-scale effective power of the pusher-barge system was calculated based on the model test total resistance at ship speed 7 knots, and frictional resistance was calculated using ITTC-1957 formula. Figure 9 shows the residual resistance coefficient based on the wetted surface area, effective power and effective power per unit barge of the various pusher-barge combinations. From the figures, the following findings have been concluded:

- Pusher-barge 4BP(2) and 6BP(3) with extended breadth in the middle and aft caused much higher residual resistance and required higher power to run at ship speed 7 knots in their respected series.
- Pusher-barge 8BP(1) with pusher located at the farthest aft of the system (longest LOA) is having higher resistance as compared to 8BP(2) and 8BP(3) with pusher located in-between and side of the barges.

To study the effect of pusher in the pusher-barge system with regards to residual resistance, a simple series of experiments were performed, as shown in Appendix A. From the experiments, it can be seen that by adding a pusher to the aft of a system, residual resistance increased. Comparison of pusher-barge 8BP(1) and 8BP(2) also found that by shortening the overall length of a pusher-barge system by moving the location of the pusher to the side of the system, residual resistance and required horse power to move the system at constant speed 7 knots decreased. However, 4BP(1) and 4BP(2) comparison reminds that if extended breadth occurs in-between the total length of the barges that blocks the water from flowing smoothly, residual resistance can increase dramatically.

In effective power comparison, for pusher-barge systems that have the same number of barges, the required effective power can be summarized as: 4BP(1) < 4BP(2), 6BP(1) < 6BP(2) < 6BP(3), 8BP(1) > 8BP(2)  $\approx$  8BP(3). Pusher-barge 8BP(2) and 8BP(3) require similar amount of power to move at ship speed 7 knots, and have the most efficient effective power per unit barge among all the eight tested pusher-barge systems.

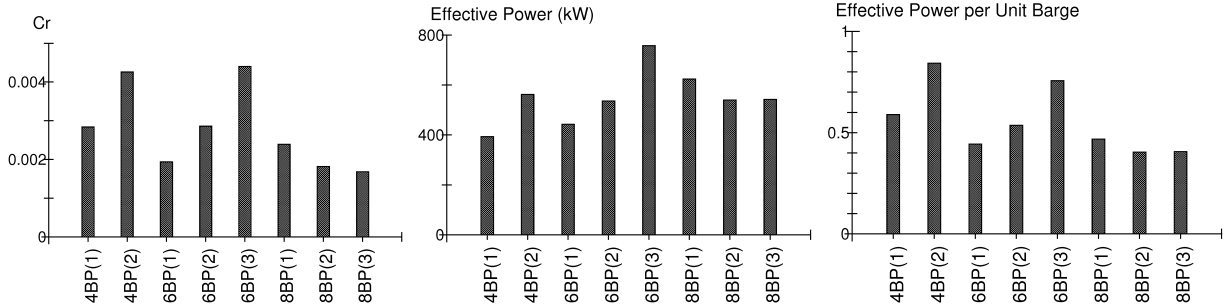


Figure 9: Residual resistance coefficient, effective power and effective power per unit barge comparisons (7 knots)

## 6 Maneuvering Simulations

### 6.1 Simulations Outline

Maneuvering motions of pusher-barge systems were simulated using a FORTRAN program written by the authors. Rudder angle used in the simulations was 20 degrees. Effect of wind, wave and current as well as shallow and restricted water effects were not taken into account in the simulations. Propeller revolution was set at 300rpm and initial forward speed of the pusher-barge system is 7 knots. In order to maintain a constant forward speed of 7 knots, controllable pitch propeller (CPP) was used in the simulation. Twin screws and twin rudders were installed at port and starboard at the aft of the pusher.

Each pusher-barge system has its own propeller pitch ratio in order to maintain a constant forward speed of 7 knots at rudder angle zero degree, but for asymmetrically arranged pusher-barge systems (8BP(1) and 8BP(2)), straight course keeping at constant speed was not achievable without the assistance of rudder control, due to the uneven force in the system. Auto-pilot was added in the simulation program

Table 5: Propeller, rudder and hull interaction parameters

symbol	value	symbol	value
$t$	0.164	$a_H$	0.194
$w_{P0}$	0.34	$t_R$	0.055
$\varepsilon$	0.987	$\gamma_R$	0.23

for these two cases, and it is found that offset rudder angle -0.6 degree (port) was needed for 8BP(1) and 3.7 degrees (starboard) was needed for 8BP(2) for straight course keeping at ship speed 7 knots.

Hydrodynamic derivatives captured from the model tests as shown in Table 3 are used in the simulation. Details of the simulation's calculations are shown in Appendix B. Propeller, rudder and hull interaction parameters used in the simulations with referred to [4] are shown in Table 5.

## 6.2 Simulations Results

Figure 13 shows the turning trajectories of the eight pusher-barge systems with 20 degrees rudder angle. For pusher-barge 8BP series, simulation of port and starboard turns are included. For symmetrically arranged pusher-barge system, only starboard turn simulation is made, except for 8BP(3) for comparison purpose with other 8BP series. Figure 14 shows the plots of advance distance and tactical diameter.

In 4BP series, it is found that when having the pusher located in-between the barges (4BP(2)), tactical diameter and advance distance reduced by a significant amount. Course stability index,  $C$ , doesn't give much information in indicating the turning behavior of 4BP series of pusher-barge system. When further studying the differences in turning performance with related to the various hydrodynamic derivatives, the authors found that some of the non-linear derivatives terms play important roles in influencing the turning performance of the pusher barge system. They are  $Y'_{\beta\beta\beta}$ ,  $Y'_{\beta\beta r}$  and  $N'_{\beta\beta r}$ . Pusher-barge 4BP(2) has a significant increment in these non-linear hydrodynamic derivatives that have high damping effect in turning, which should lead to bigger turning circle of 4BP(2). However, the results shown otherwise. Hence, the authors checked the rudder force of 4BP series and found that 4BP(2) has very high rudder force difference than 4BP(1) (Figure 10). The higher rudder force has lead to the reason of smaller turning circle of 4BP(2), which cancel out the high damping effect from the non-linear hydrodynamic derivatives in 4BP(2).

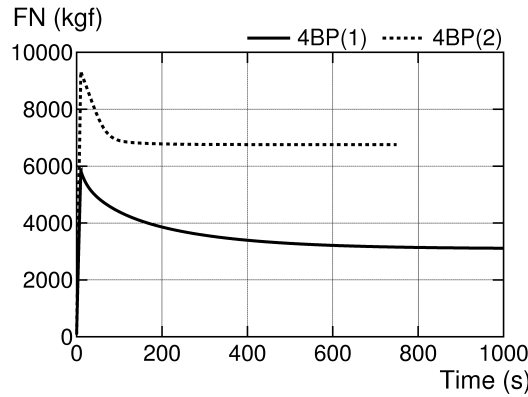


Figure 10: Rudder force is 4BP series

In 6BP series, 6BP(3) with triangle type of arrangement gives the smallest value of tactical diameter and advance distance. Course stability index,  $C$ , plays an important role in indicating the turning performance of the system in 6BP series. The smaller the value of  $C$ , the better the turning performance (smaller turning circle). 6BP(3) has the smallest value of  $C$ , followed by 6BP(2) and then 6BP(1). Another factor that contributes to the small turning trajectory of pusher-barge 6BP(3) is the relatively high resistance in pusher-barge 6BP(3) and high pitch ratio that directly resulted in high rudder force in pusher-barge 6BP(3) as compared to 6BP(2) and 6BP(1). The big rudder force in 6BP(3) has caused turning of 6BP(3) to be much more efficient than the rest. Rudder force comparison of 6BP series is shown in Figure 11.

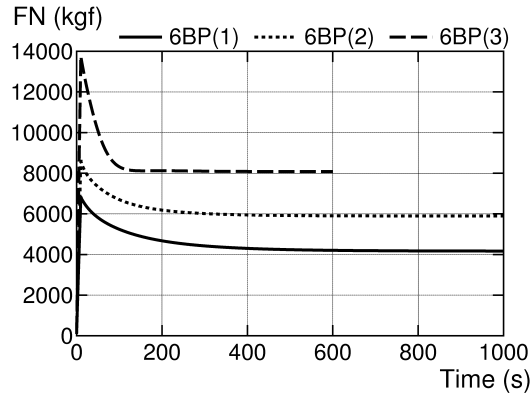


Figure 11: Rudder force is 6BP series

In analysing the results of 8BP series, the authors took pusher-barge 33BP from [1] to compare with 8BP(1) due to their similar arrangements. Plot comparison of the two systems is shown in Figure 12. From the figure, it is found that pusher-barge 8BP(1) has very similar turning trajectory as 33BP in port side turning. This finding matches well with the straight course moving test that has been conducted by the authors earlier in the simulations in finding the pitch ratio of 8BP(1), where rudder offset of 8BP(1) is very minor (0.6 degree to port), showing that the asymmetry effect of pusher-barge 8BP(1) is very little. In starboard side turning, the asymmetry effect gives more influence by having a significant reduction in turning trajectory. In pusher-barge 8BP(2), due to the stronger asymmetry effect (rudder offset of 3.7 degrees starboard in straight course moving test), pusher-barge 8BP(2) makes larger port side turning and smaller starboard side turning than pusher-barge 8BP(1). Turning trajectory of pusher-barge 8BP(3) increased significantly as compared to 8BP(1) and 8BP(2). Course stability index,  $C$ , doesn't give much info in showing the differences in turning trajectories in 8BP series, hence analysis were shifted to individual hydrodynamic derivatives of the various pusher-barge systems. In 8BP series, the authors found that for pusher-barge 8BP(3), non-linear derivatives  $Y'_{\beta\beta\beta}$ ,  $Y'_{\beta\beta r}$  and  $N'_{\beta\beta r}$  increased significantly. These non-linear derivatives give high damping effect in turning motion, which are the main cause to the significant increment in turning trajectory of pusher-barge 8BP(3).

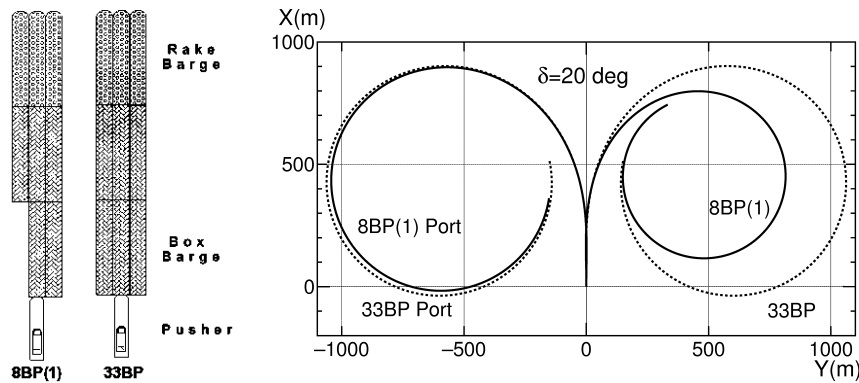


Figure 12: Turning trajectories of 8BP(1) and 33BP [1]

Asymmetrical arrangement of the pusher-barge systems resulted asymmetrical hull force for port and starboard sides. In asymmetrical cases, when arrangement is weighted on the one side, the system tends to make bigger turning trajectory on the opposite side, and vice versa. As a consequences to this, pusher-barge 8BP(1) and 8BP(2) produce different port and starboard turning trajectories.

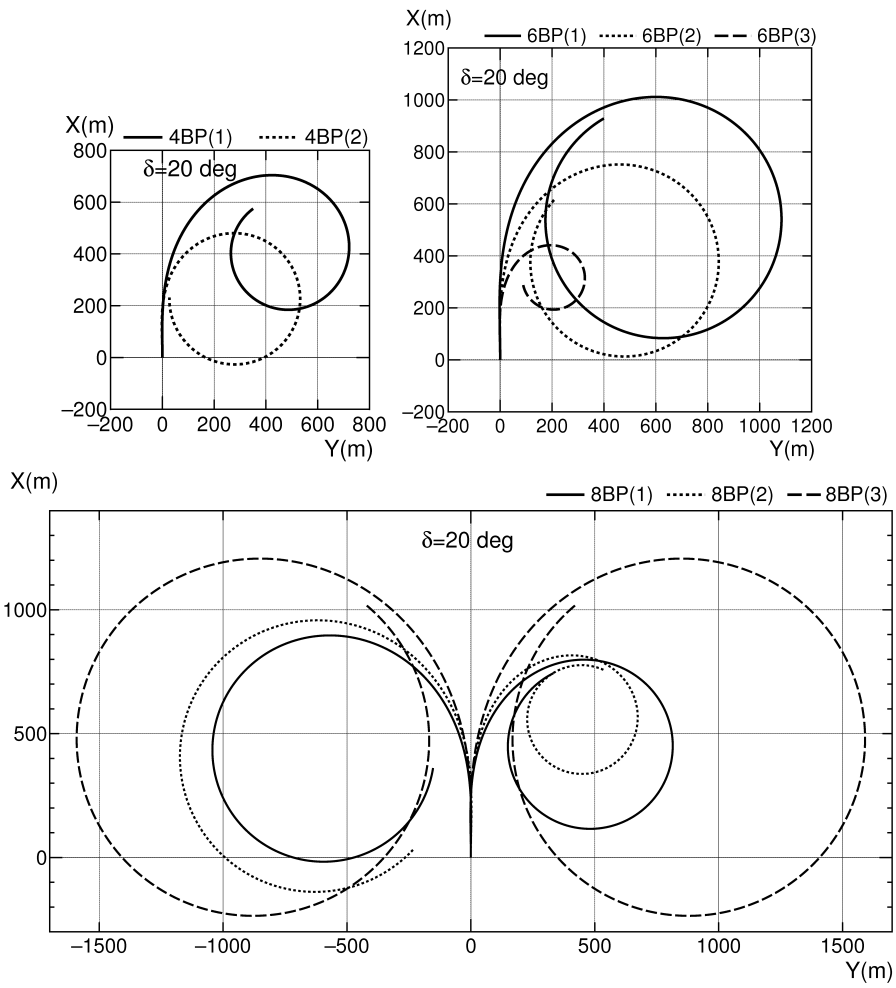


Figure 13: Turning trajectories ( $\delta = 20^\circ$ )

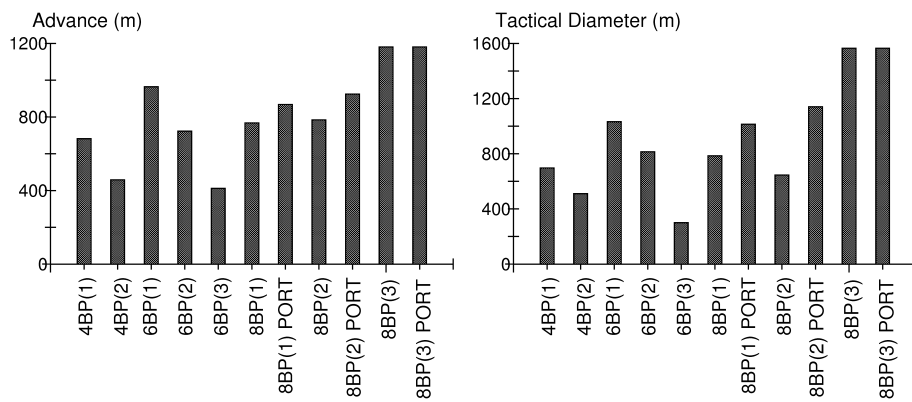


Figure 14: Tactical diameter and advance distance ( $\delta = 20^\circ$ )

## 7 Concluding Remarks

Model experiments of eight different pusher-barge systems were carried out in Hiroshima University Towing Tank. Hydrodynamic derivatives were obtained from the experiment data and computer simulation was performed based on the obtained hydrodynamic derivatives.  $Y'_0$ ,  $Y'_{\beta\beta}$ ,  $N'_0$ , and  $N'_{\beta\beta}$  were added in the force and moment equations in order to fit model test data more accurately for asymmetrically arranged pusher-barge systems. For pusher-barge system with pusher located in-between the barges, not at the farthest aft of the system (4BP(2), 8BP(2) and 8BP(3)), are unstable in course keeping (negative course stability index,  $C$ ). Pusher-barge system with pusher located in-between the barges (8BP(2) and 8BP(3)) have lower residual resistance and required less power to operate at ship speed 7 knots as compared to 8BP(1). Pusher-barge 4BP(2) on the other hand has higher resistance as compared to 4BP(1) due to the extension of width in the middle of the system. Similar case happened to pusher-barge 6BP(3). Breadth extension in the middle of a pusher-barge system should be avoided.

In the computer simulations, uneven force on port and starboard were taken into consideration in calculating the added mass and total moment of a pusher-barge system. Rudder force and non-linear hydrodynamic derivatives ( $Y'_{\beta\beta\beta}$ ,  $Y'_{\beta\beta r}$  and  $N'_{\beta\beta r}$ ) play important roles in influencing the turning trajectory of a pusher-barge system. In some cases, course stability index ( $C$ ) gives good information in indicating the turning performance, where there smaller the value of  $C$ , the better the turning performance. For asymmetrically arranged pusher-barge system, pusher-barge that has arrangement weighted on one side will have larger turning trajectory when making an opposite turn. Asymmetrically arranged pusher-barge system will also have a different port and starboard turning performance, due to the asymmetry propeller and rudder forces (8BP(2)) and asymmetry hull force (8BP(1) and 8BP(2)).

For future work, the authors suggest conducting captive model test to capture the value of propeller, rudder and hull interaction parameters (current values are based on assumptions). Full-scale tests data will be a good credit and comparison to the simulation results if performed.

## References

- [1] Koh KK, Yasukawa H, Hirata N, Kose K (2008) Maneuvering simulations of pusher-barge systems. J Mar Science Tech (to be published)
- [2] Yasukawa H, Hirata N, Koh KK, Punayangkool K, Kose K (2007) Hydrodynamic force characteristics on maneuvering of pusher-barge systems (in Japanese). J Jpn Soc Nav Archit Ocean Eng 5:133-142
- [3] Pfennigstorf J (1970) Handbuch der Werften X Band. Bearb von K Wendel. Schiffahrts-Verlag HANSA, C Schroedter & Co, Hamburg 11
- [4] Yoshimura Y, Sakurai H (1989) Mathematical model for the manoeuvring ship motion in shallow water (3rd Report) (in Japanese). J Kansai Soc Nav Archit Jpn 211
- [5] Hirano M (1980) On the calculation method of ship maneuvering motion at the initial design phase (in Japanese). J Soc Nav Archit Jpn 147:144-153
- [6] Fujii H, Tuda T (1961) Experimental research on rudder performance (2) (in Japanese). J Soc Nav Archit Jpn 110:31-42
- [7] Yoshimura Y, Nomoto K (1978) Modeling of maneuvering behaviour of ships with a propeller idling, boosting and reversing (in Japanese). J Soc Nav Archit Jpn 144:57-69

## A Effect of Pusher on Overall Pusher-Barge System's Resistance

Figure 15 shows comparison of the resistance of 4 different pusher-barge systems (with and without pusher). Pusher-barge 1B is to be compared with 1BP, and pusher-barge 2B is to be compared with 2BP. The combinations have been tested in Hiroshima University towing tank at ship's speed 7 knots, with frictional resistance calculated using ITTC 1957 formula and residual resistance is then obtained. Comparison of residual resistance coefficient ( $C_r$ ) based on wetted surface area is plotted in Figure 16. From the figure, it is found that by having pusher at the back of the barges, residual resistance increased by around 20-25%.

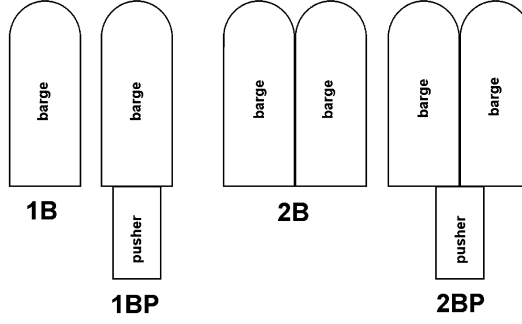


Figure 15: Pusher-barge systems with and without pusher

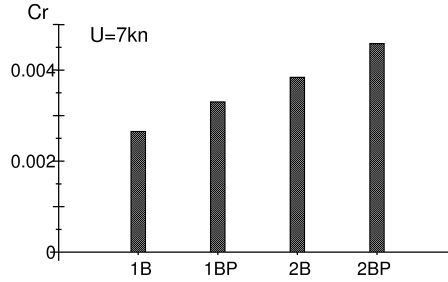


Figure 16: Residual resistance coefficient comparison

## B Maneuvering Motions Simulation for Asymmetrically Arranged Pusher-Barge System

Figure 17 shows the coordinate systems used in the paper.  $O - X_0Y_0Z_0$  are the space coordinate system, with  $X_0Y_0$  referring to the water surface and  $Z_0$  vertically downwards from the water surface.  $\psi$  is the angle from  $X_0$  to the position of the ship.  $G - xyz$  is the ship's coordinate system, where  $G$  is the center of gravity of the ship,  $x$  is the forward direction of the ship and  $y$  is the lateral direction of the ship.  $xy$  plan forms the water surface where the ship is located, and  $z$  is the vertical downwards direction from the center of gravity of the ship. Maneuvering motions of the pusher-barge system (surge, sway, yaw) are defined in the motion equations shown in Equation (9). In the equation,  $u$  is the forward speed,  $v$  is the lateral speed,  $r$  is the turning rate,  $m$  is the mass of the ship, and  $I_{zz}$  is the moment of inertia of the ship.  $m_{ij}$  ( $i = 1, 2, 6; j = 1, 2, 6$ ) is the added mass and added moment of inertia of the pusher-barge system that occur when a ship accelerate or decelerate or in turning motion. On the right hand side of the equations,  $X$  is the total forward force,  $Y$  is the total lateral force and  $N$  is the total moment at the center of gravity of the pusher-barge system.

$$\left. \begin{aligned} (m + m_{11})\dot{u} - (m + m_{22})vr + m_{12}\dot{v} + m_{16}\dot{r} &= X \\ (m + m_{11})ur + (m + m_{22})\dot{v} + m_{12}\dot{u} + m_{26}\dot{r} &= Y \\ (I_{zz} + m_{66})\dot{r} + m_{16}\dot{u} + m_{26}\dot{v} &= N \end{aligned} \right\} \quad (9)$$

$X$ ,  $Y$ , and  $N$  are the forces and moment introduced from hull ( $H$ ), propeller ( $P$ ) and rudder ( $R$ ), which are expressed in Equation (10).

$$\left. \begin{aligned} X &= X_H + X_P + X_R \\ Y &= Y_H + Y_R \\ N &= N_H + N_R - (Y_H + Y_R)x_G - X_P y_P - X_R y_R \end{aligned} \right\} \quad (10)$$

In model tank test, measurement was done at the midship of the pusher-barge system, while longitudinal force  $X$  is unaffected, but lateral force  $Y$  and moment  $N$  need to be corrected from midship to the center of gravity of the pusher-barge system. The relationship of the lateral velocity at midship  $v_m$  to the lateral velocity at center of gravity of the pusher-barge system  $v$  is shown in Equation (11). The midship drift

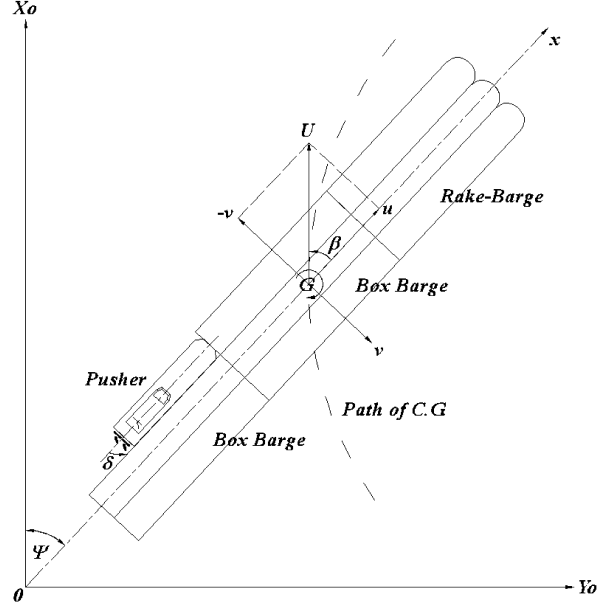


Figure 17: Coordinate systems

angle  $\beta_m$  is defined in Equation (12).

$$v_m = v - x_{G^*} r \quad (11)$$

$$\beta_m = \tan^{-1} \left( \frac{-v_m}{u} \right) \quad (12)$$

Hydrodynamic force that acts on a hull when a ship makes a diagonal turn is mainly caused by the dynamic pressure of the fluid. If the flow along a hull is to be related to the ship's length, and the displacement of the hull is to be related to the draught of the ship, then the relationship of the flow and pressure can be related to  $LOA \times d$ . Hydrodynamic force  $(X_H, Y_H, N_H)$  on ship's hull based on the above consideration is shown in Equation (13). In the equation,  $U$  is the ship's speed ( $U = \sqrt{u^2 + v^2}$ ), and  $X'_H, Y'_H, N'_H$  are defined in Equation (7).

$$\left. \begin{aligned} X_H &= (1/2)\rho LOA dU^2 X'_H(\beta_m, r') \\ Y_H &= (1/2)\rho LOA dU^2 Y'_H(\beta_m, r') \\ N_H &= (1/2)\rho LOA^2 dU^2 N'_H(\beta_m, r') \end{aligned} \right\} \quad (13)$$

Propeller of a ship is assumed to be fixed at aft and only contributing force in the  $X$  direction. Total force produced by a propeller as experienced by a ship is defined as:

$$X_P = (1 - t) \sum T \quad (14)$$

where  $t$  is the thrust deduction factor and  $\sum T$  is the total thrust produced by the propellers (twin screws in this study).

$$T = \rho n_P^2 D_P^4 K_T(J_P, p) \quad (15)$$

In Equation (15)  $D_P$  is the propeller diameter,  $K_T$  is the thrust coefficient,  $J_P$  is the propeller advanced coefficient, and  $p$  is the propeller pitch ratio.  $K_T$  and  $J_P$  are defined in Equation (16) and Equation (17).

$$K_T(J_P, p) = -0.3260pJ_P - 0.2005J_P + 0.5234p - 0.0398 \quad (16)$$

$$J_P = \frac{u(1 - w_P)}{n_P D_P} \quad (17)$$

In Equation (17),  $w_P$  is the propeller wake fraction factor which changes accordingly with the drift angle  $\beta$  and also the ship turning rate  $r'$ . Hirano's formula [5] was used in calculating the wake fraction factor.

$$w_P = w_{P0} \exp[C_1 \beta_P^2] \quad (18)$$

where  $w_{P0}$  is the wake factor during the forward motion of the pusher-barge system,  $\beta_P$  is the drift angle at the propeller position ( $\equiv \beta - \ell'_P r'$ ), and  $C_1$  is the correction factor.  $\ell'_P$  is the ratio of the position of propeller location to the center of gravity of the pusher-barge system with forward direction in positive value to the length overall of the pusher-barge system.

Rudder forces ( $X_R$  and  $Y_R$ ) and moment ( $N_R$ ) are defined in Equation (19).

$$\left. \begin{aligned} X_R &= -(1 - t_R) \sum F_N \sin \delta \\ Y_R &= -(1 + a_H) \sum F_N \cos \delta \\ N_R &= -(x_R + a_H x_H) \sum F_N \cos \delta \end{aligned} \right\} \quad (19)$$

where  $\delta$  is the rudder angle,  $t_R$ ,  $a_H$  and  $x_H$  are the rudder and hull interaction parameters, and  $x_R$  is the  $x$ -coordinate point on which the rudder force  $Y_R$  acts.  $x_H$  is assumed to be  $0.85x_R$ .  $F_N$  is defined as below:

$$F_N = \frac{1}{2} \rho A_R U_R^2 f_\alpha \sin \alpha_R \quad (20)$$

In the equation,  $A_R$  is rudder area and  $f_\alpha$  is gradient of the lift coefficient of the rudder.  $f_\alpha$  is estimated using Fujii's formula[6].  $U_R$  is the flow velocity to the rudder and  $\alpha_R$  is the effective rudder in-flow angle:

$$U_R = \sqrt{u_R^2 + v_R^2} \quad (21)$$

$$\alpha_R = \delta - \tan^{-1} \left( \frac{v_R}{u_R} \right) \quad (22)$$

In Equation (21),  $u_R$  is the water flow speed towards the rudder and  $v_R$  is the lateral flow speed after passing the propeller.  $v_R$  is calculated using Equation (23) which is related to the rudder location and is influenced by the flow entrance angle to the rudder  $\beta_R$  ( $\equiv \beta - \ell'_R r'$ ), and  $\gamma_R$  is the flow-rectification coefficient to the rudder.  $\ell'_R$  is the ratio of the effective rudder position to the center of gravity of the pusher-barge system with forward direction in positive value to the length overall of the pusher-barge system.  $\ell_R$  is assumed to be  $2x_R$ .

$$v_R = U \gamma_R \beta_R \quad (23)$$

$u_R$  is defined using Yoshimura's formula[7]:

$$u_R = \frac{\varepsilon u_P}{1 - s} \sqrt{1 - 2(1 - \eta \kappa)s + 1 - \eta \kappa(2 - \kappa)s^2} \quad (24)$$

where  $s$  is the propeller slip ratio,  $\eta$  is the ratio of propeller diameter with rudder height,  $\kappa$  is the propeller flow correction factor ( $\kappa = 0.6/\varepsilon$  is normally used), and  $\varepsilon$  is the flow coefficient of the rudder with respect to its location.